Complete identification of products of the reaction 20Ne + 12C at 110 Mev

J. Menet, A.J. Cole, N. Longequeue, J.J. Lucas, G. Mariolopoulos, J.B. Viano, J.C. Saulnier, D.H. Koang

Classification
Physics Abstracts
25.70

COMPLETE IDENTIFICATION OF PRODUCTS OF THE REACTION $^{20}Ne + {}^{12}C$ AT 110 MeV

J. MENET, A. J. COLE, N. LONGEQUEUE, J. J. LUCAS, G. MARIOLOPOULOS, J. B. VIANO, J. C. SAULNIER and D. H. KOANG

Institut des Sciences Nucléaires (IN2P3 et USMG)
B.P. 257, Centre de Tri, 38044 Grenoble Cedex, France

(*Reçu le 2 mai 1977, accepté le 18 mai 1977*)

Résumé. — L'identification complète des produits de la réaction ^{20}Ne (110 MeV) + ^{12}C a été faite en utilisant un temps de vol et un télescope $\Delta E - E$. Les distributions angulaires des produits de réaction et leur spectre en énergie étaient obtenus à des angles compris entre 3,7° et 17° (Lab). La section efficace mesurée des résidus d'évaporation est de 1 270 ± 150 mb. L'analyse des résultats a été faite en utilisant un formalisme Hauser-Feshbach dépendant du moment angulaire.

Abstract. — Complete identification of products of the reaction ^{20}Ne (110 MeV) + ^{12}C has been carried out using time of flight and $\Delta E - E$ measurements. Angular distributions of reaction products and energy spectra were obtained between laboratory angles of 3.7° and 17°. The evaporation residue cross-section was measured to be 1 270 ± 150 mb. Analysis of the data has been carried out using the Hauser-Feshbach angular momentum dependent formalism.

Nuclear reactions $^{12}C(^{20}Ne, X)$ $E = 110$ MeV. Simultaneous identification in mass and charge. Measured yields, energy spectra and angular distributions for $6 < A < 32$. Evaporation analysis.

1. **Introduction.** — Increasing attention has been focused recently on composite systems produced in reactions between heavy ions [1]. Measurements of the cross-section for formation of a compound system as a function of energy have been used to explore the fusion barrier [2] and the results have been interpreted in terms of a critical angular momentum [3] or a critical radius [4] beyond which no compound nucleus formation takes place. In heavy and medium-weight composite systems some study has been made of strongly inelastic processes [5, 6] including fission [7] and quasi-fission [8, 9] which together with complete fusion and direct reactions make up the total reaction cross-section. The strongly inelastic processes become more important with increasing bombarding energy.

The simple method of measuring fusion cross-sections in which individual reaction products are not identified [2] encounters serious difficulties if applied to light composite systems since evaporation residues following compound nucleus formation may be confused with products of strongly inelastic collisions. The situation is improved by identification of mass or charge of the products [9, 10] since the energy spectra for fusion products are centered almost exactly around the energy corresponding to the velocity of the recoiling nucleus. Furthermore, data obtained in this way may be compared to fusion evaporation calculations using statistical models. A further considerable improvement is, of course, obtained if charge and mass are identified both from the point of view of statistical model predictions and for the identification of the mechanism responsible for low yield products which may otherwise be obscured by neighbouring isotopes (isotones).

Up to the present, few articles have appeared in the literature in which complete identification of both mass and charge was made. Apart from the work of the Strasbourg group [11] we know of only one such publication [12]. In this work Weidinger *et al.* measured energy spectra at angles between 2° and 22° for two reactions : $^{16}O + {}^{16}O$ and $^{16}O + {}^{12}C$ at an incident ^{16}O energy of 60 MeV. Cross-sections, energy spectra, and angular distributions of the completely identified product nuclei were compared to Hauser-Feshbach calculations. Overall good agreement was obtained using the level density parameters of Gilbert and Cameron [19]. However the cross-sections for evaporation residues for the lightest nuclei observed

were not well predicted and the predicted angular distributions were also disappointing. The bombarding energy was low enough so that little contribution was seen from processes other than direct reactions and compound nucleus formation. Nevertheless, from the point of view of the statistical analysis, the results clearly showed the need for complete identification of the products. Furthermore, the double humped structure produced in energy spectra at small laboratory angles due to the evaporated alpha particles would probably not have been observed had only charge been identified.

We report in this paper the first of a series of measurements on the $^{20}Ne + {}^{12}C$ system with complete identification of the reaction products. Some measurements including charge identification already exist [22] at 80 MeV and the elastic scattering has been studied quite extensively [14]. The experiments were begun in the hope of obtaining information on nuclear level densities for light nuclei. Furthermore the strongly inelastic processes in light systems have as yet received little attention. Thus our aim is to understand the fusion process at relatively low energies in order to extrapolate this understanding to higher energies where non compound processes are expected to become important. It should also be interesting to compare the systems $^{20}Ne + {}^{12}C$ and $^{16}O + {}^{16}O$ although the detailed comparison will require data over a wide energy range for the two systems. We describe here the measurement and analysis of the $^{20}Ne + {}^{12}C$ reaction at 110 MeV incident Ne energy. The experimental arrangements are described in section 2 and the results in section 3. The analysis of that part of the cross-section attributed to compound nucleus formation is given in section 4. Finally, section 5 summarizes our main conclusions and directions for further study.

2. **Experimental method.** — The experiment was carried out by directing a 110 MeV ^{20}Ne beam from the Grenoble cyclotron onto a self supporting carbon target (200 $\mu g/cm^2$) on which was evaporated 8 $\mu g/cm^2$ of gold. Absolute cross-sections in the ^{20}Ne-^{12}C reaction were obtained by normalizing the data to the elastic (assumed to be Rutherford) scattering on the gold layer, the thickness of which was measured by comparing the elastic scattering with that from a reference (100 $\mu g/cm^2$) gold target.

Beam currents were measured in a Faraday cup of internal diameter 12 mm covering an angle of $\pm$ 3°, which was sufficient to accept the collimated beam in the scattering chamber. The target thickness was monitored during the experiment using a detector situated at 17° to count elastic events relative to Faraday cup counts.

The detection system was mounted on a rotatable arm connected to the scattering chamber via a sliding seal. Identification of 20 nuclei $6 < A < 32$ was accomplished by measurement of time of flight t, energy loss, ΔE, and residual energy, E. The ΔE detector consisted of an ionization chamber of 100 mm length filled with an argon-methane mixture (90 % Ar, 10 % CH_4) at a pressure of 40 mm of Hg. The chamber entrance window was made of a 40 $\mu g/cm^2$ formvar foil mounted on a metallic grid which transmitted 85 % of the incident particles. The E measurement was accomplished using a low-resistivity silicon detector of 200 μm thickness and 450 mm^2 surface area.

The time-of-flight of the reaction products was measured over a flight path of 292 cm. The start signal was produced by a channel electron multiplier which detected electrons liberated by the passage of a heavy ion through two 10 $\mu g/cm^2$ carbon foils (Fig. 1). Electrons were accelerated between the foils and the tube by a 1 kV electrostatic potential. The rise time of this device was typically 6 ns. The stop signal was taken from the E detector which was mounted at the back of the ionization chamber.

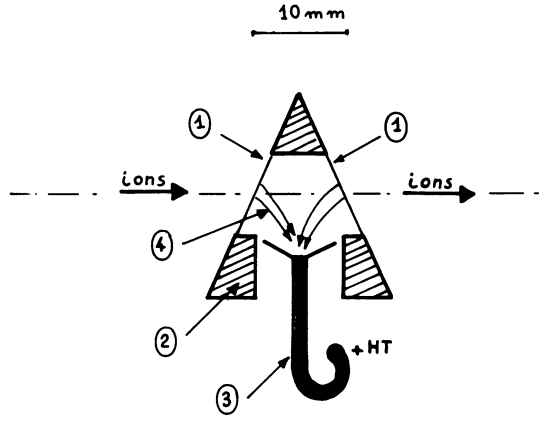

FIG. 1. — Start detector. 1) 10 $\mu g/cm^2$ carbon foils at a potential of 1 kV. 2) Prism supporting the foils. 3) Electron channel multiplier operating at 3 kV. 4) Trajectories for electrons ejected from the carbon foils during the passage of reaction products. The electrons are accelerated by the 1 kV potential between the foils and the collecting cone of the electron multiplier.

The solid angle of the detection system was limited by the ionization chamber entrance window. The carbon foils were large enough in area so as to average out small angle scattering gains and losses at the ΔE entrance window. Likewise the E detector was large enough to detect any particle passing through the ΔE detector.

The electronics were set up before the experiment using a ^{244}Cm α source (10^6 counts/s into 4 π). The time resolution was $\sim$ 1.2 ns for these α particles (5.8 MeV) and approximately 700 ps for the elastically scattered ^{20}Ne.

The detection angle was determined to within 0.2° by comparing the energy difference between the elastic scattering from the carbon and gold of the target. The electronic stability was monitored by observing ΔE, E and t peaks corresponding to elastic scattering from the gold target layer in a multichannel analyser. An on-line computer system was used to calculated the square of the particle velocity v^2, $(E + \Delta E)\, t^2$ (mass),

and $\Delta E + \mu E$ where μ was chosen so that $\Delta E + \mu E$ was approximately constant for a given nuclear charge Z. The mass and charge information was displayed as a function of v^2 in a biparametric representation during each run (Fig. 2). Finally the quantities E, $\Delta E + \mu E$, t, $(E + \Delta E)\, t^2$, and v^2 were stored on magnetic tape. The mass resolution for particles of 2 MeV/nucleon was $\Delta M/M = 1.7 \times 10^{-2}$ and the charge resolution, $\Delta Z/Z = 3.5 \times 10^{-2}$ (Fig. 3).

FIG. 2. — Example of biparametric spectrum. *a*) Charge identification $\Delta E + \mu E$ *versus* v^2. *b*) Mass identification $(\Delta E + E)\, t^2$ *versus* v^2.

From the biparametric representations (Fig. 2) it was an easy matter to set mass and charge limits for each nucleus. With these limits the magnetic tapes were processed for the energy spectra of each nucleus. A low energy cut-off of 0.6 MeV/nucleon imposed by the ΔE detector was apparently sufficiently low so that all the cross-section was effectively measured. The incident $^{20}Ne^{5+}$ (110 MeV) beam was contaminated by 5 % of $^{16}O^{4+}$. Using experimental results for ^{16}O on ^{12}C (60 MeV) we have estimated that this contamination does not introduce more than a 5 % error in the measured residue cross-sections. The ^{16}O and ^{20}Ne elastic peaks permitted the absolute calibration of the ΔE and E detectors.

3. **Experimental results.** — 3.1 CRITICAL ANGULAR MOMENTUM. — Measurements were carried out between 3.7° and 17° in the laboratory. Energy spectra at 4.2° are shown in figure 5. Identification of the evaporation residue part of the cross-section was made from the form of the energy spectra and angular distributions. This procedure was particularly important for ^{20}Ne and ^{24}Mg. ^{24}Mg could be produced either by α particle transfer or by fusion followed by evaporation of two alphas or one alpha and four nucleons. The fusion evaporation contribution was centered around the energy corresponding to the velocity of the recoiling compound nucleus. We therefore assumed that the high energy peak in the ^{24}Mg spectrum (Fig. 5*c*) corresponded to an α transfer with a Q value of ~ -15 MeV. This contribution

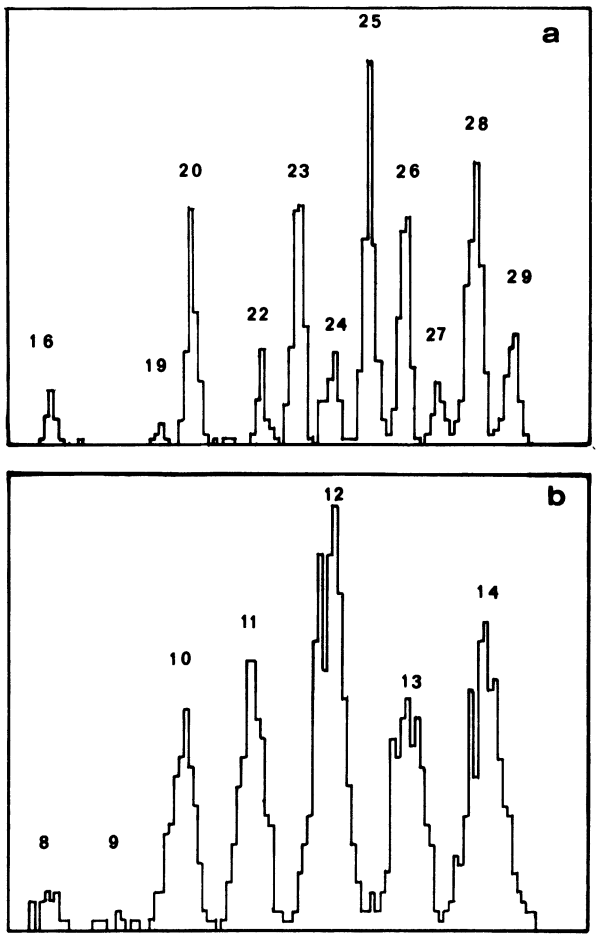

FIG. 3. — Typical spectrum of mass and charge identification at 6° lab for v^2 corresponding to the average velocity of the recoiling compound nucleus ^{32}S.

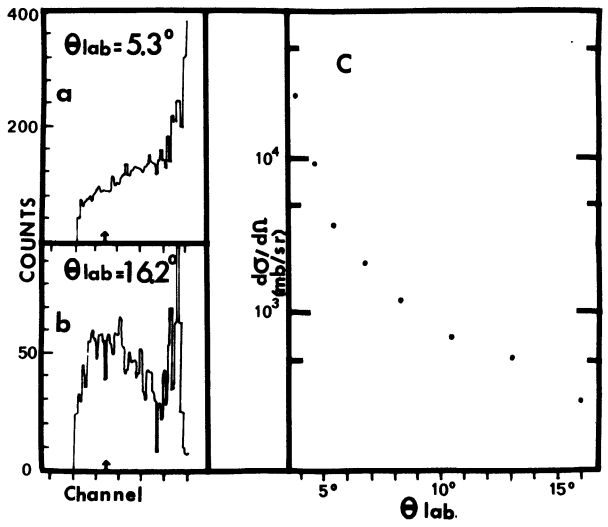

FIG. 4. — ^{20}Ne energy spectra (a, b) and angular distribution (c). The arrows in the energy spectra indicate the energy corresponding to the velocity of the recoiling ^{32}S nucleus.

integrated over the angular distribution amounted to 24 mb. The ^{20}Ne energy spectra were more difficult to interpret. At large angles a fusion evaporation contribution was clearly distinguishable (Fig. 4*b*) but at small angles this component was obscured by a

featureless energy distribution extending from the elastic peak down to the experimental low energy out off (Fig. 4*a*). The evaporation residue contribution was estimated by using the shape of the angular distributions from neighbouring isotopes to extrapolate the residue cross-section to small angles. The value obtained was 200 ± 50 mb (^{20}Ne).

The total evaporation residue cross-section was obtained by summing all the evaporation residue reaction products for $A \geqslant 20$. The value obtained was $\sigma_{ER} = 1\,270 \pm 150$ mb. The measured cross-sections for each isotope are given in table I. Practically

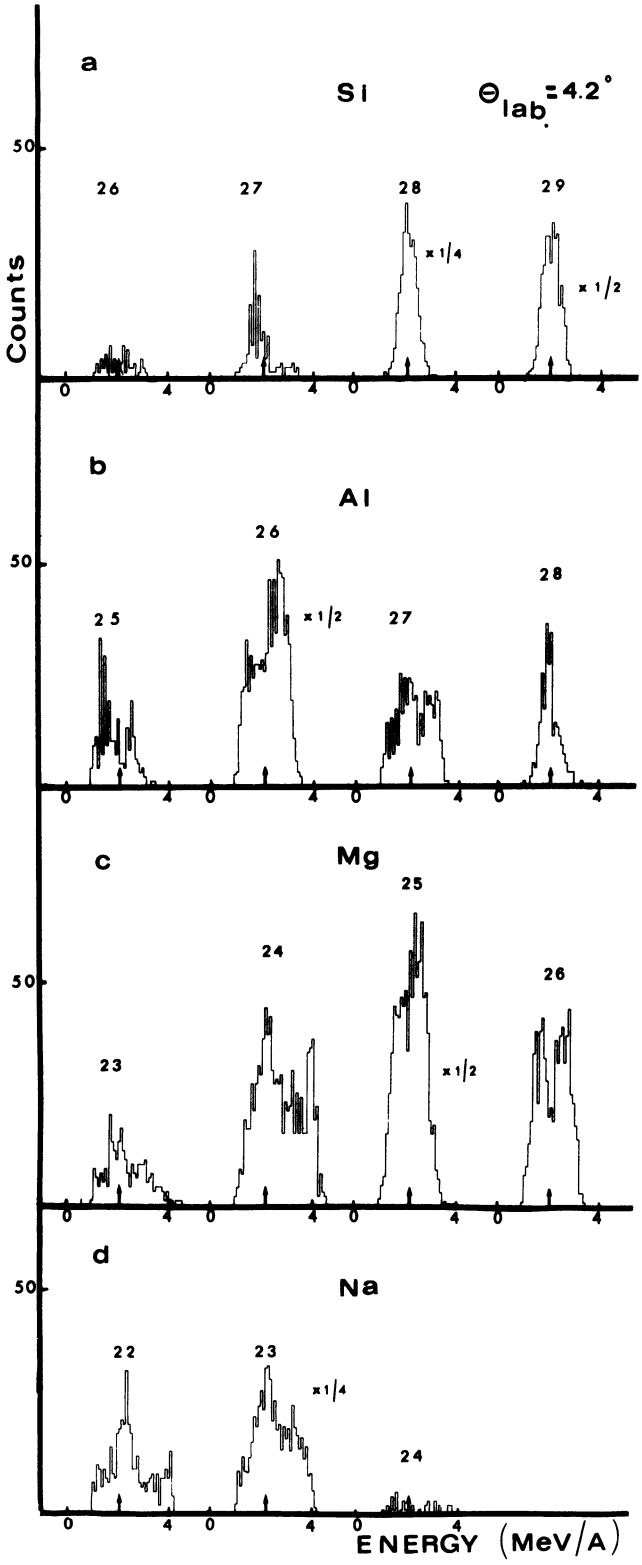

FIG. 5. — Recoiling nuclei energy spectra at a laboratory angle of 4.2°. In the figure the arrows indicate the energies corresponding to the compound nucleus recoil velocity.

TABLE I

Partial evaporation residue cross-sections, in millibarns

M \ Z	15	14	13	12	11	10	9
19					< 0.2	9	4
20				< 0.2	< 1	200	4
21				< 1	4	11	
22			1	5	36	11	
23			5	38	210	6	
24		< 0.2	10	83	5	< 1	
25		< 1	26	163	3		
26		5	161	70	< 1		
27	< 0.2	10	42	5			
28	2.5	68	16	< 1			
29	2.5	35	4				
30	< 1	1.5					
31	< 0.2						
32							

no cross-section was found for masses < 20 with the exception of ^{16}O coming from the beam contamination or from α transfer. Integration of all reaction products excluding the ^{20}Ne elastic cross-section gave a value for the total reactions cross-section of $\sigma_R = 1\,700 \pm 170$ mb. If, as seems probable, the evaporation residue cross-section is equal to the compound nucleus formation cross-section, we deduce a value of the critical angular momentum for compound nucleus formation in the sharp cut off model of $l_{cr} = 23$. An optical model calculation using the energy dependent potential parameters of Vandenbosch [14] gives $\sigma_R = 1\,806$ mb at 110 MeV in good agreement with our experimental value. We note that 75 % of the total cross-section at 110 MeV corresponds to fusion and that most of the remaining cross-section corresponds to inelastic ^{20}Ne events.

3.2 ENERGY SPECTRA (Fig. 5). — We observe essentially two main types of energy spectra for evaporation. The first, corresponding to nucleon evaporation, consists of a bell shaped structure centered around the value E_R corresponding to the compound nucleus recoil velocity. The second, which is more pronounced at small angles, consists of a double humped structure again centered around E_R and corresponding to events in which an α emission in the forward or backward direction [12] and this structure is gradually lost as the observation angle is increased. Nucleons evaporated before or after alphas do not alter the separation between the peaks but some attenuation of the

observed structure is produced. This is due to the relative smallness of the recoil momentum produced by nucleon evaporation as compared with α evaporation. These conclusions are generally confirmed by detailed calculations (section 4) and are extremely useful since they allow qualitative conclusions to be made simply by examination of the residue energy spectra. Their application may be illustrated with reference to figure 5 which shows energy spectra measured at $\theta_{lab} = 4°2$.

Si (Fig. 5*a*) : four principal isotopes $^{26,27,28,29}Si$ were observed. All spectra are centered around E_r. The ^{28}Si spectrum, which is similar to that of ^{29}Si, is characteristic of nucleon evaporation since no structure is observed ([1]). Furthermore single α evaporation from ^{32}S would produce ^{28}Si excited well above the particle emission threshold. In contrast, ^{26}Si and ^{27}Si appear to contain a strong α-nucleon evaporation component.

Al (Fig. 5*b*) : again four principal isotopes $^{25,26,27,28}Al$ were observed. The ^{28}Al spectrum is, as expected, characteristic of nucleon evaporation while the mass 25 and 26 products show the typical α-nucleon form. The non characteristic form of the ^{27}Al spectrum suggests contributions from both α-nucleon and five nucleon processes.

Mg (Fig. 5*c*) : four isotopes $^{23,24,25,26}Mg$ were observed. The masses 26, 25 are characteristic of α-nucleon processes. The energy spectra of the masses 24 and 23 are not characterized by any simple form. Indeed the situation is rather complex since a 2 α process may contribute. In this case the angular distributions for each of the evaporated α particles may play an important role in determination of the final residue energy spectrum. In the case of ^{24}Mg the situation is further complicated by an α transfer contribution.

Na (Fig. 5*d*) : we observed principally two isotopes $^{22,23}Na$. Both have energy spectra extending over a wide energy range and centered roughly around E_R. A high energy shoulder is apparent in the ^{23}Na spectrum. The non-symmetrical character of these spectra indicate that at least one α was evaporated in the de-excitation process.

3.3 ANGULAR DISTRIBUTIONS. — The experimental angular distributions for the most abundant product nuclei are shown in figure 6. The widths of the angular distributions increase with the difference between the mass of the observed residue and the compound nucleus, due to the increase in the transverse momentum transferred to the residue during the evaporation process. Exceptions to this rule can however occur when α emission competes with 4 nucleon emission.

An exception to the general form of the measured angular distributions occurs for ^{20}Ne (Fig. 4*c*). At large angles (between 8° and 16°) the ^{20}Ne angular distribution resembles that of neighbouring isotopes. However at small angles figure 4 shows that the cross-section rises rapidly and is apparently not characteristic of a fusion evaporation process. In fact, the angular distribution resembles that of deep inelastic reactions seen in other studies [9].

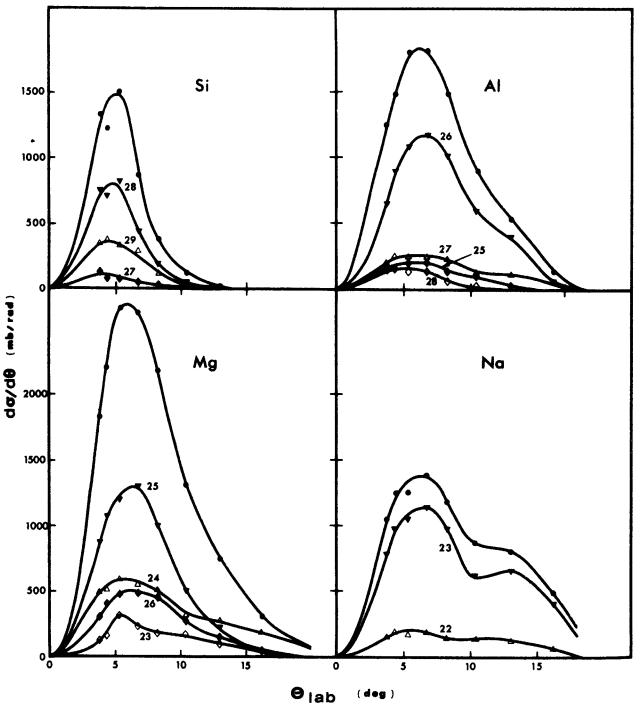

FIG. 6. — Experimental angular distributions. The solid lines which have been drawn to guide the eye suggest that the cross sections $d\sigma/d\theta$ go to 0 at 0°. As discussed in the text this is not necessarily true. In each case the upper curve represents the summed cross-section.

4. Analysis. — 4.1 PROGRAMME PARAMETERS AND ISOTOPIC DISTRIBUTIONS. — The analysis of our experimental results was carried out using the evaporation code GROGI 2 of Grover and Gilat [13]. The use of this programme which, at each evaporation step, carries out an angular momentum dependent Hauser-Feshbach calculation has been described in reference [12]. The calculations permit evaporation of neutrons, protons, α particles, and γ rays. At each evaporation step the program requires specification of level densities in each daughter nucleus and corresponding transmission coefficients, T_l, for particle emission. Widths for dipole and quadrupole γ ray emission are also required.

The population in angular momentum space of the compound nucleus was obtained using a sharp cut-off model. Thus the partial cross-sections for compound nucleus formation were taken as $\sigma_l = \pi\lambda^2(2l + 1)$ for $l \leqslant l_{cr}$ and $\sigma_l = 0$ for $l > l_{cr}$. The critical angular momentum l_{cr} was obtained from the measured fusion cross-section using the same model :

$$\sigma_F = \pi\lambda^2(l_{cr} + 1)^2 .$$

Our measured value of $\sigma_F = 1\,270$ mb yields $l_{cr} = 23$.

([1]) This was also the case in the work of Weindinger *et al.* [12].

TABLE II

Optical model potential parameters

Projectile	Target	Energy (MeV)	V_R MeV	R_R fm	A_R fm	W_V MeV	R_V fm	A_V fm	W_D MeV	R_D fm	A_D fm	V_{so} MeV	R_{so} fm	A_{so} fm	R_C fm	Ref.
—	—	—	—	—	—	—	—	—	—	—	—	—	—	—	—	—
^{20}Ne	^{12}C	110	17.0	1.35 (*)	0.57	23.26	1.35 (*)	0.57	0			0			1.35 (*)	[14]
n	$20 \leqslant A \leqslant 31$	$0 < E < 25$	$56 - 0.32\,E + 12\,\eta$	1.17	0.75	$0.22\,E - 1.56$	1.26	0.58	$13.0 - 0.25\,E - 12\,\eta$	1.26	0.58	6.2	1.01	0.75		[15]
p	$20 \leqslant A \leqslant 31$	$0 < E < 25$	$54 - 0.32\,E + 0.4\,\varepsilon + 24\,\eta$	1.17	0.75	$0.22\,E - 2.7$	1.32	$0.51 + 0.7\,\eta$	$11.8 - 0.25\,E + 12\,\eta$	1.32	$0.51 + 0.7\,\eta$	6.2	1.01	0.75	1.17	
α	$A = 27, 28$	$1 < E < 50$	165.0	1.45	0.52	19.0	1.45	0.52	0			0			1.45	[16]
α	$20 \leqslant A \leqslant 26$	$1 < E < 50$	171.0	1.52	0.52	19.0	1.52	0.52	0			0			1.52	[17]
α (**)	$20 \leqslant A \leqslant 28$	$1 < E < 50$	165.0	2.0	0.52	19.0	2.0	0.52	0			0			1.45	

$$\eta = \frac{N - Z}{A}\,;\ \varepsilon = \frac{Z}{A^{1/3}}\,.$$

(*) Potential radius = $1.35(20^{1/3} + 12^{1/3})$ fm.

(**) The arrows on figure 6 corresponds to calculations with this α potential, obtained by arbitrarly increasing the radius parameter of reference [16].

Some justification for the sharp cut-off approximation was provided by an optical model calculation using the energy dependent parameters of Vandenbosch *et al.* [14] at 110 MeV. The calculated T values differ from unity by not more than 1 % up to $l = 23$.

The transmission coefficients at each evaporation step for nucleons were calculated using the energy dependent parameters of Becchetti and Greenless [15]. The α parameters which were assumed to be energy independent, were taken from references [16] and [17]. All optical model parameters are summarized in table II. The γ widths were normalized in the same way as in reference [12] : thus the reduced width was taken to be 0.3 eV for a dipole transition and 0.01 eV for a quadrupole transition at 8 MeV excitation. Test calculations showed that predictions were somewhat insensitive to these parameters.

Level densities were calculated using the formula proposed by Lang [18] which is written in terms of a level density parameter, a, and a spin parameter R such that $aR = 2\,I/\hbar^2$ where I is the moment of inertia of the nucleus considered. For a we have used the Gilbert and Cameron [19] approximation

$$\frac{a}{A} = 0.12 + 0.009\,17\,S\,,$$

where A is the nucleus mass number and S is a shell correction. Values of S were obtained when possible from reference [19] and were otherwise extrapolated from the tabulated values. The Yrast energies below which the level density is zero for a given J were either calculated from the formula

$$E = \frac{J(J+1)\,h^2}{2\,I} + \delta$$

or for low energies taken from experiment [20]. δ is the pairing correction tabulated in reference [19]. The parameter R was fixed by requiring that the moment of inertia was that of a rigid sphere :

$$I = \frac{2}{5} M r_0^2\, A^{2/3}\,.$$

There is some evidence [21] in fusion experiments on light nuclei that the limit to compound nucleus formation at a given excitation energy is given by the Yrast line i.e. $l_{cr} = l_{YRAST}$. Since a measurement of the fusion cross-section for ^{20}Ne on ^{12}C has been made at 80 MeV [22] we have supposed that the l_{cr} obtained from this work corresponds to l_{YRAST} at the corresponding excitation energy of 49 MeV. With this supposition we find $r_0 = 1.3$ fm.

We remark that the calculations are extremely sensitive to the positions of the Yrast line. Thus a calculation made using the liquid drop moment of inertia [23] failed to account even qualitatively for our data. Essentially this failure was due to high level densities which produce enhanced nucleon emission on the first evaporation step.

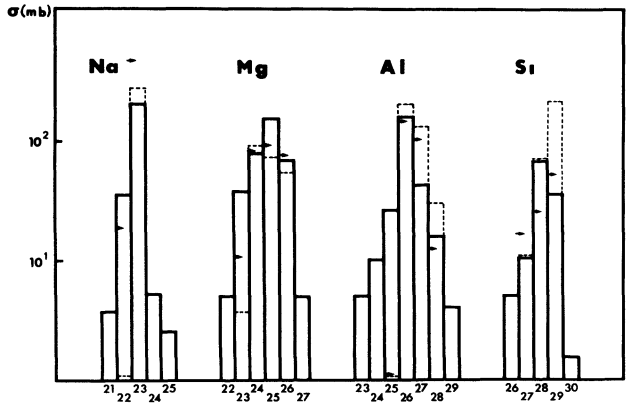

FIG. 7. — Experimental cross-sections for the principal isotopes (full lines). The arrows and dashed lines are the results of different calculations using the GROGI 2 code as explained in the text.

As can be seen in figure 7 (dotted lines) the measured cross-sections are qualitatively reproduced by the calculations. A detailed description of the evaporation chains leading to each product is given in table III. The observed discrepancies seem to be due (as noted in ref. [12]) to an underestimation of the α/nucleon evaporation ratio. Thus somewhat better agreement was obtained by increasing the α optical potential radius thus reducing the Coulomb barrier and increasing the corresponding transmission coefficients. (These calculations are indicated by arrows in figure 7.) However no detailed exploration of the parameter space was carried out. There are two reasons for this. Firstly the calculations are rather long and expensive. Secondly, as will be seen in the following section, it is impossible at present to use measured angular and energy distributions in order to constrain the parameters of the model.

4.2 ENERGY SPECTRA AND ANGULAR DISTRIBUTIONS. — In principle, measurement of energy spectra and angular distributions provide strong constraints on predictions of evaporation models. However, the construction of these quantities from the evaporation model predictions presents a number of problems. Firstly, for each evaporation in a given chain, the angular distribution of the evaporated particles varies in principle with its energy [24]. Since GROGI 2 does not predict angular distributions, it is necessary to assign some arbitrary angular distribution to each evaporated particle in the chain. Secondly the construction of the resultant center of mass recoil momentum for more than one evaporation is somewhat lengthy and involves introduction of further hypotheses expressing the fact that the evaporations cannot be considered as independant events. These constraints should properly be applied to both the energy and the angular momentum populations.

In this first article we avoid these problems by adopting the philosophy of reference [12]. Thus, explicitly, we assume isotropic c.m. angular distributions for the evaporated particles. In this case the resultant centre of mass recoil momentum for two successive evaporations may be written as :

$$\frac{H(p)}{p} = \iint \frac{H_1(p_1)}{p_1} \frac{H_2(p_2)}{p_2} \, dp_1 \, dp_2$$

where $H_1(p_1)$ and $H_2(p_2)$ are respectively the momentum spectra for the first and second evaporations. The condition of non independance of successive evaporations was expressed by requiring that the final nucleus is left at a positive or zero excitation energy. Thus for two evaporations, we have :

$$E_x - (E_1 + E_2) > Q_1 + Q_2$$

where

E_x : excitation energy in the compound nucleus,

E_1 : kinetic energy of the first particle in c.m. system,

TABLE III

Details of calculated evaporation chains

Nuclei	Formation process and % of calculated cross-section	σ (mb)
^{29}Si	pnp : 32.3, ppn : 54.5, npp : 13.2	227
^{28}Si	α : 4.1, ppnn : 52.9, pnpn : 23.9, pnnp : 6.8, nppn : 11.1	67
^{27}Si	αn : 84.5, nα : 15.5	10
^{28}Al	pppn : 41.0, ppnp : 35.1, pnpp : 16.4, nppp : 7.5	30
^{27}Al	αp : 77.4, pα : 22.6	136
^{26}Al	αpn : 43.6, αnp : 7.9, pαn : 27.8, pnα : 11.2, npα : 7.0, nαp : 2.5	214
^{26}Mg	αpp : 47.3, pαp : 37.3, ppα : 15.4	55
^{25}Mg	αppn : 10.8, αpnp : 18.2, αnpp : 4.1, pαpn : 12.5, pαnp : 20.8, ppαn : 8.1, ppnα : 17.0, nαpp : 2.2, npαp : 2.9, nppα : 3.4	71
^{24}Mg	αα : 100.0	83
^{23}Mg	ααn : 32.0, αnα : 49.0, nαα : 19.0	4
^{23}Na	ααp : 58.5, αpα : 25.9, pαα : 15.6	292

E_2 : kinetic energy of the second particle in c.m. system,

Q_1 and Q_2 : Q values corresponding respectively to the first and second evaporations.

The formula may be iterated provided the above constraint can be modified to take account of a third evaporation. We have included such a modification by requiring that the parent nucleus, after the second evaporation, has an excitation energy sufficiently high so that evaporation of a third particle (with an average energy given by the evaporation model) leaves the final nucleus at a positive (or zero) excitation energy. Thus for three evaporations we require :

$$E_x - (E_1 + E_2 + \bar{E}_3) \geqslant Q_1 + Q_2 + Q_3$$

where

$\bar{E}_3$: mean energy of the third particle,

Q_3 : Q value corresponding to the third evaporation.

The transformation of $H(p)$ to the laboratory system permits calculations of energy spectra and angular distributions. Examples of energy spectra are shown in figure 8. The calculations lend support for the qualitative conclusions made in section 3. However, the predictions are somewhat disappointing in detail. The prediction shown in figure 8 for ^{26}Al may be improved by assigning, as in reference [12], a non isotropic angular distribution to the c.m. resultant recoil momentum. We feel it is rather difficult to justify such a procedure since the degree of anisotropy is unknown. It is possible for example to obtain

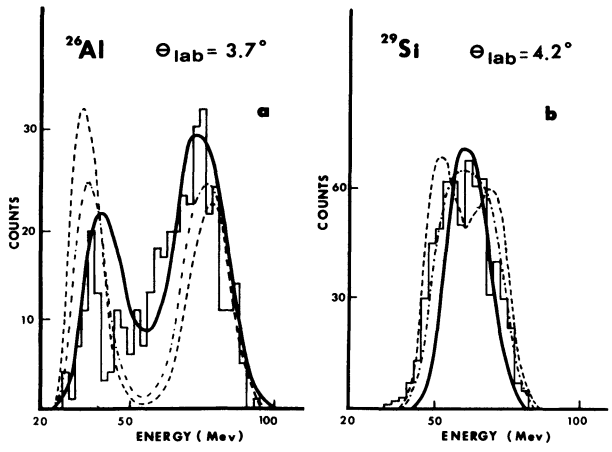

FIG. 8. — Energy spectra and calculations for isotropic c.m. recoil (full line), 1/sin θ recoil (dot-dashed line) and 1/sin^2 θ recoil (dashed line).

resultant recoil angular distributions with an anisotropy greater than the 1/sin θ limit usually assumed for single evaporations. Furthermore of course, as mentioned above the anisotropy depends in principle on the energy (energies) of the evaporated particle (particles). Figures 8, 9 show the effect of increasing the anisotropy of the c.m. angular distributions for the case of ^{29}Si and ^{26}Al for both small angle energy spectra and angular distributions. An important

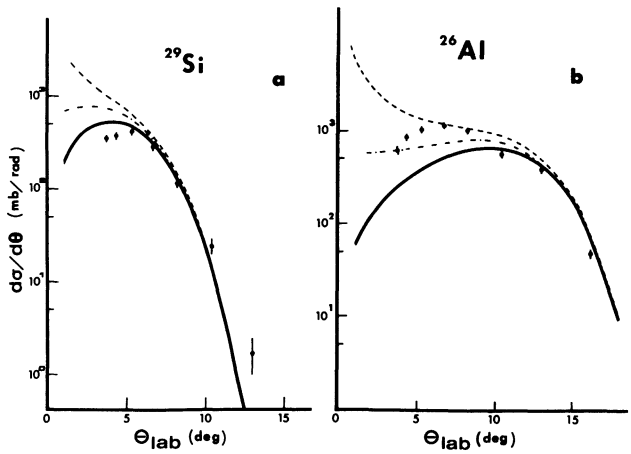

FIG. 9. — Angular distributions and calculations for isotropic c.m. recoil (full lines), 1/sin θ recoil (dot-dashed line) and 1/sin^2 θ recoil (dashed lines).

remark should be made in this context, i.e. for a resultant recoil momentum with a 1/sin θ or more anisotropic angular distribution, the laboratory cross-section $d\sigma/d\theta_{lab}$ does not go to zero at $\theta_{lab} = 0$ as is sometimes assumed in evaluation of fusion cross-sections. An allowance for this effect has been included in our estimate of the fusion cross-section error.

As far as detailed comparison of our measured angular distributions with evaporation model predictions is concerned, our conclusion is that such a comparison is not useful unless the construction of the resultant recoil angular and momentum c.m. distribution is carried out correctly within the context of the model. In particular we consider it impossible to decide if the discrepancies obtained in this work and in some cases in reference [12] are due to failure of the evaporation model or to approximations subsequently introduced in the calculations.

In summary detailed conclusions concerning angular and energy distributions must await the development of more sophisticated methods of analysis.

5. **Summary and conclusions.** — In this article we have presented results on the simultaneous charge and mass identification of reaction products from 110 MeV ^{20}Ne bombardment of ^{12}C. Energy spectra, angular distributions and cross-sections for 20 isotopes have been obtained. Apart from the isotopes ^{16}O, ^{20}Ne and ^{24}Mg, the observed spectra are characteristic of a fusion evaporation mechanism. The measured reaction cross-section is in good agreement with the optical model prediction and the measured fusion cross-section leads to a value of $l_{cr} = 23\ \hbar$ in the sharp cut-off model. The measured isotopic distribution are in qualitative agreement with angular momentum dependent Hauser-Feshbach model predictions. Such models may be used to deduce properties of highly excited nuclei with large angular momentum.

The data are extensive and in principle provides severe constraints on model calculations. However at the present time the available methods of analysis are

not sufficiently sophisticated to enable a thorough exploitation of the measurements. In this context a Monte Carlo calculation would be of considerable value provided the proper inclusion of the angular distribution of the evaporated particles at each evaporation step is not too time consuming.

Finally there is strong indication in the ^{24}Mg and ^{20}Ne spectra of a contribution from a highly inelastic process. For ^{20}Ne the observed cross-section for the process is 400 mb. However we see no marked variations of the angular distributions of the non fusion cross-section as a function of energy and it is thus not evident that this process is the same deep inelastic scattering observed at higher energies and for heavier projectile target combinations.

In our opinion measurements at other energies both above and below 110 MeV should be made and analyzed more thoroughly in the context of the statistical model. We also expect an increase in non fusion processes at higher energies. Such measurements, when combined with those reported here, should provide severe tests of proposed level densities in light nuclei as well as information on non-compound processes in light systems which at the present time is rather scarce.

Acknowledgments. — Our deepest thanks go to M. Pierre Oustric who provided the technical support for the experiment and in particular constructed the detection system. We would also like to thank members of the PDP computing team for invaluable assistance with data acquisition and reduction programmes. Finally we thank Dr. Ed. Gross for a careful reading of the manuscript.

References

[1] LEFORT, M., *Rep. Progr. Phys.* **39** (1976) 129.
[2] SCOBEL, W., MIGNEREY, A., BLANN, M. and GUTBROD, M., *Phys. Rev.* **C 11** (1975) 1701.
[3] WILCZYNSKI, J., *Nucl. Phys.* **A 216** (1973) 386.
GROSS, D. H. E. and KALINOWSKI, H., *Phys. Lett.* **48B** (1974) 302.
BASS, R., *Phys. Lett.* **47B** (1973) 139.
[4] GLAS, D. and MOSEL, U., *Nucl. Phys.* **A 237** (1975) 429.
GALIN, J., GUERREAU, D., LEFORT, M. and TARRAGO, X., *Phys. Rev.* **C 9** (1974) 1018.
[5] GALIN, J., Physique Nucléaire avec des Ions Lourds, Caen 1976, *J. Physique* **37** (1976) C 5 and references contained therein.
[6] MORETTO, L. G., GALIN, J., BABINET, R., FRAENKEL, Z., SCHMITT, R., JARED, R. and THOMPSON, S. G., *Nucl. Phys.* **A 259** (1976) 173 and references contained therein.
[7] BARETTE, G., BRAUN-MUNZINGER, P., GELBKE, C. K., GROSSE, E., HARNEY, H. L., KUZMINSKI, J., TSERRUYA, I. and WALCHER, T. H., *Z. Phys.* **A 274** (1975) 121.
[8] HANAPE, F., LEFORT, M., NGO, C., PETER, J. and TAMAIN, B., *Phys. Rev. Lett.* **32** (1974) 738.
[9] NATOWITZ, G. B., NAMBOODIRI, M. N., EGGERS, R., GONTHIER, P., GEOFFREY, K., HANUS, R., TOWSLEY, C. and DAS, K., *Nucl. Phys.* **A 277** (1977) 477.
[10] PUHLHOFER, F., PFEFFER, W., KOHLMEYER, B. and SCHNEIDER, W. F. W., *Nucl. Phys.* **A 244** (1975) 329.
[11] COFFIN, J. P., Proc. Colloque Franco-Japonais, Dogashima, sept. 1976, p. 160 and COFFIN, J. P., ENGELSTEIN, P., GALLMANN, A., HEUSCH, B., WAGNER, P. and WEGNER, H. E. (to be published).
[12] WEIDINGER, A., BUSCH, F., GAUL, G., TRAUTMANN, W. and ZIPPER, W., *Nucl. Phys.* **A 263** (1976) 511.
[13] Computer Programme GROGI 2. See
GROVER, J. R. and GILAT, J., *Phys. Rev.* **157** (1967) 802.
[14] VANDENBOSCH, R., WEBB, M. P. and ZISMAN, M. S., *Phys. Rev. Lett.* **33** (1974) 842.
[15] BECCHETTI, F. D. and GREENLEES, G. W., *Phys. Rev.* **182** (1969) 1190.
[16] WUHR, W., HOFMANN, H. and PHILIPP, G., *Z. Phys.* **269** (1974) 365.
[17] EBERHARD, K. A. and ROBSON, D., *Phys. Rev.* **C 3** (1971) 149.
[18] LANG, D. W., *Nucl. Phys.* **77** (1966) 545.
[19] GILBERT, A. and CAMERON, A. G. W., *Can. J. Phys.* **43** (1965) 1446.
[20] ENDT, P. M. and VAN DER LEUN, *Nucl. Phys.* **A 214** (1973). AZENBERG-SELOUE, F., *Nucl. Phys.* **A 190** (1972).
[21] STOKSTAD, R. G., GOMEZ DEL CAMPO, BIGGERSTAFF, J. A., SNELL, A. H. and STELSON, P. H., *Phys. Rev. Lett.* **36** (1976) 1529.
[22] CONJEAUD, M., GARY, S., HARAR, S., LOISEAUX, J. M., MENET, J. and VIANO, J. B., *European Conference on Nuclear Physics with heavy Ions*, Caen 1976, Communications, p. 125.
[23] COHEN, S., PLASIL, F. and SWIATECKI, W. I., *Ann. Phys.* (N.Y.) **82** (1974) 557.
[24] See for example
THOMAS, T. D., *Ann. Rev. Nucl. Sci.* **18** (1968) 343.